Modifying Adaptive Cruise Control Systems for String Stable Stop-and -Go Wave Control

Fangyu Wu, Joy Carpio, Matthew Bunting, Matthew Nice, Daniel Work, Jonathan Sprinkle, Jonathan Lee, Sharon Hornstein, and Alexandre Bayen, *Fellow, IEEE*

***Abstract*—This letter addresses the important issue of energy inefficiency and air pollution resulting from stop-and-go waves on highways by introducing a novel controller called the Attenuative Kerner's Model (AKM). The objective of AKM is to enhance an existing Adaptive Cruise Control (ACC) system to improve vehicle following in stop-and-go waves. It is designed as a hybrid controller that is compatible with a wide range of commercial vehicles equipped with ACC. The article demonstrates the *local* string stability of the controller. Next, it presents a comparative analysis of AKM against two benchmarks: a human driver and a commercial ACC system, through numerical simulations and physical experiments using a 2022 Cadillac XT5. The findings reveal that AKM substantially outperforms both the human driver and the ACC in controlling low-speed, stop-and-go waves. The results indicate that AKM could act as an additional control layer for existing ACC systems, potentially improving their operational efficiency and reducing pollution emissions, thus contributing to more sustainable highway transportation.**

***Index Terms*—Autonomous vehicle navigation, energy and environment-aware automation, stop-and-go wave control.**

I. Introduction

RECENT traffic monitoring efforts have revealed the prevalence of stop-and-go waves on freeways. Initial investigations examined these waves [15], albeit with limitations due to the dataset's length and duration, which constrained understanding of their prevalence. Wu [36] demonstrated the propagation and dissipation of stop-and-go waves over extended periods using aerial drone videos in afternoon rush hours on commute highways. Gloudemans [4] showed that during congestion periods, stop-and-go waves persist, moving at regular speeds and propagating through the traffic in a direction opposite to the flow, consistently observed throughout the congestion periods on all monitored days.

This phenomenon can be attributed to human driving dynamics, even in the absence of bottlenecks [28], or it can be induced by the unstable behavior of commercial Adaptive Cruise Control (ACC) systems [6]. When equipped with properly designed ACC systems, particularly those that are string stable [30], one can attenuate stop-and-go waves, leading to a reduction in fuel consumption and emissions. For example, previous studies have shown a reduction in fuel consumption of nearly 40% as reported in [27], and a reduction in emissions ranging between 15% and 73% as quantified in [26].

Such results underscore the importance of considering the role that Adaptive Cruise Control (ACC) might play in promoting sustainable highway transportation practices. Given that a significant portion of ACC systems on the road are potentially string instable [6], there is merit in retrofitting these legacy ACC systems on the roads.

However, existing literature has not given enough consideration in this aspect. Common ACC methods involve the manipulation of acceleration commands [1], [11], [13], [17]. However, by design, ACC systems are intended to accept velocity commands. In addition, optimization-based and flow-based methods frequently require wireless communications and costly onboard computing [5], [20], [23], [32], [35]. Such hardware requirements are often unattainable for earlier automobiles. Furthermore, learning-based methods inherently function as black boxes [9], [21], [34]. This characteristic complicates the verification of string stability, a crucial factor given the safety-critical nature of driving.

Therefore, developing a method that can provably stabilize stop-and-go waves and is widely compatible with a broad range of commercial vehicles equipped with ACC is crucial. To address these challenges, we introduce a string stable ACC method that overcomes issues of backward compatibility. Building upon the acceleration-based Kerner's model [11], we propose a novel velocity-based controller, named the *Attenuative Kerner's Model* (AKM).

We summarize the main contributions of our work below.

1) We have developed a novel ACC controller, which is a modification of Kerner's model [11] and is compatible with a wide range of ACC systems.
2) We demonstrate the *local* string stability of the Attenuative Kerner's Model through frequency-domain analysis.

Manuscript received 4 March 2024; accepted 28 July 2024. Date of publication 8 August 2024; date of current version 22 August 2024. This article was recommended for publication by Associate Editor A. Thakur and Editor A. Banerjee upon evaluation of the reviewers' comments. This work was supported in part by the National Science Foundation under Grant CNS-1837244 and in part by the U.S. Department of Energy's Office of Energy Efficiency and Renewable Energy (EERE) under Award CID DE-EE0008872. *(Corresponding author: Fangyu Wu.)*

Fangyu Wu, Jonathan Lee, and Alexandre Bayen are with the University of California, Berkeley, Berkeley, CA 94720 USA (e-mail: fangyuwu@berkeley.edu).

Joy Carpio is with the University of California, Berkeley, Berkeley, CA 94720 USA, and also with National University Manila, Manila 1008, Philippines.

Matthew Bunting, Matthew Nice, Daniel Work, and Jonathan Sprinkle are with the Vanderbilt University, Nashville, TN 37212 USA.

Sharon Hornstein is with the General Motors, Herzliya 4672513, Israel.

Digital Object Identifier 10.1109/LRA.2024.3440834

3) We benchmark our controller against both a human driver and an OEM ACC controller, employing both simulation and field tests for comprehensive comparison.

II. Related Works

Stop-and-go waves are a traffic phenomenon commonly emerged on congested highways. They can be triggered by the presence of a road bottleneck, e.g., a drop in speed limit or a reduction in lane capacity, or arise naturally due to the inherent instability in human car-following behavior. String stability has been introduced and is utilized to qualitatively assess the presence of instability in car-following dynamics [30]. The oscillatory dynamics observed in this experiment were later modeled as analogs to gas-dynamical detonation waves [3], enabling researchers to explore how these waves could be dampened. Sugiyama [28] provided the first closed-course experimental validation, demonstrating the existence of stop-and-go waves resulting from unstable human car-following behavior. Gunter [6] demonstrated through field experiments that such unstable car-following dynamics could also be present in commercial ACC systems.

Traditionally, control theory researchers have been exploiting the robotic nature of cars as both sensors and actuators to stabilize car-following. On a microscopic level, a classical approach to stabilizing car-following involves optimizing parameters of car-following models as demonstrated in [13], [29]. Another strategy involves construction of explicit feedback control mechanisms focusing on gap regulation and speed tracking [1], [11], [17]. Furthermore, there are studies that apply model predictive control to design implicit feedback controllers by leveraging additional non-local information [5], [23], [35]. On a macroscopic level, alternative methods to mitigate traffic congestion include the adaptation of infrastructure compliance, such as dynamically setting speed limits based on downstream traffic conditions [20], [32].

Meanwhile, machine learning, particularly reinforcement learning, has emerged as an alternative approach to wave smoothing, with many instances showing promising empirical performance. The early adoption of reinforcement learning for adaptive cruise control is documented in [19]. More recent explorations in this area are detailed in [9], [21], [34]. While these modern methods excel at utilizing both synthetic and real-world data to enhance performance, their certification for string stability remains challenging due to the opaque nature of black-box neural networks.

Parallel to controller design, experimental work is also essential, particularly in assessing the robustness of proposed solutions. The challenge of implementing precise acceleration-based feedback control arises from the often noisy nature of odometry or IMU measurements [25]. Additionally, Rajamani [22] demonstrated that the integration of various time delays from each sensor could lead to instabilities if the controller is not designed to accommodate them. Therefore, conducting experimental evaluations is vital to confirm the practicality of a proposed ACC method.

On the side of field experimentation, an early experiment by Stern [27] aimed to mitigate stop-and-go waves through the control of a single vehicle on a circular, single-lane road. More recently, the significant decrease in equipment costs has enabled coordinated experiments on multi-lane highways, such as those described in [14], [16].

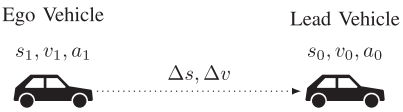

Fig. 1. Illustration of the two-vehicle car-following problem. The ego vehicle needs to follow the lead vehicle as smoothly as safety permits.

III. Attenuative Kerner's Model

Consider the two-vehicle car-following setup, as depicted in Fig. 1. At any given moment t, the lead vehicle's position, velocity, and acceleration are denoted by $s_0(t)$, $v_0(t)$, and $a_0(t)$, respectively, while those for the ego vehicle are similarly represented by $s_1(t)$, $v_1(t)$, and $a_1(t)$. The relative distance and velocity between the vehicles are defined as $\Delta s(t) := s_0(t) - s_1(t)$ and $\Delta v(t) := v_0(t) - v_1(t)$. The goal is to control the ego vehicle's behavior to ensure it follows the lead vehicle safely and smoothly in stop-and-go traffic conditions.

Given that all ACC systems on the market accept a set speed as the control input, designing a controller that outputs a velocity command ensures the highest compatibility. Therefore, building upon Kerner's model [11], we introduce the AKM as follows:

$$u_{\text{AKM}}(\Delta s, v_0, v_1) = \begin{cases} v_0 + \delta_-(\Delta s, v_1), & \Delta s \in S_-(v_1), \\ v_0, & \Delta s \in S_{\text{eq}}(v_1), \\ v_0 + \delta_+(\Delta s, v_1), & \Delta s \in S_+(v_1), \end{cases} \tag{1}$$

where

$$\begin{aligned} \delta_-(\Delta s, v_1) &= \max(a_1 \Delta s / q(v_1) + b_1, d_1), \\ \delta_+(\Delta s, v_1) &= \min(a_2 \Delta s / q(v_1) + b_2, d_2), \\ S_-(v_1) &= \{\Delta s \in \mathbb{R}_{\geq 0} : \Delta s / q(v_1) < h_-\}, \\ S_+(v_1) &= \{\Delta s \in \mathbb{R}_{\geq 0} : \Delta s / q(v_1) > h_+\}, \\ S_{\text{eq}}(v_1) &= \mathbb{R}_{\geq 0} \setminus (S_-(v_1) \cup S_+(v_1)), \\ q(v_1) &:= \max(v_1, v_{\min}), \end{aligned} \tag{2}$$

for some parameters $a_1, a_2, b_1, b_2, d_1, d_2, h_-, h_+$, and $v_{\min}$. At start-up, we set $u_{\text{AKM}}(t_0) = v_0(t_0)$.

The parameters a_1, b_1, and d_1 in $\delta_-(\cdot)$ govern the negative velocity compensation, prompting the ego vehicle to decelerate and increase the space headway. Conversely, the parameters a_2, b_2, and d_2 in $\delta_+(\cdot)$ govern the positive velocity compensation, encouraging the ego vehicle to accelerate and decrease the space headway. A graphical representation of the velocity compensation terms is depicted in Fig. 2(a). The parameters h_- and h_+ represent the minimum and maximum space headways, respectively, where $h_- < h_+$. These parameters are used to track the lead vehicle's speed. Finally, the parameter $v_{\min}$ defines the minimum velocity threshold critical for a meaningful time headway.

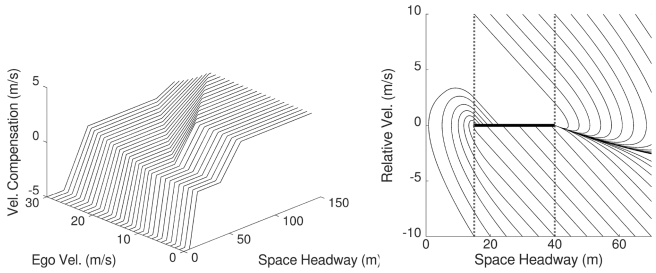

(a) Speed compensation (b) Phase portrait

Fig. 2. Speed compensation and phase portrait of the AKM with parameters in Table I.

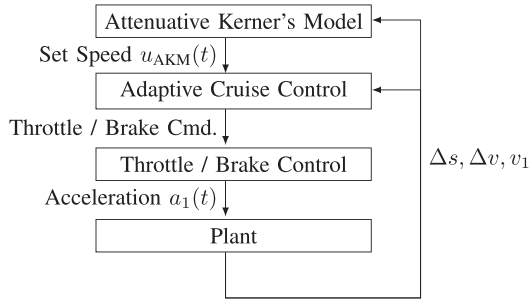

Fig. 3. Block diagram of a typical vehicle system integerated with the AKM controller.

The three switch conditions of the AKM aim to smooth oscillations in the lead vehicle's speed while maintaining a reasonable space headway between the two vehicles. When $\Delta s \in S_-$, indicating that the space headway is too small, the controller commands a speed lower than that of the lead vehicle to increase the gap. When $\Delta s \in S_+$, indicating that the space headway is too large, the controller commands a speed higher than the speed of the lead vehicle to reduce the gap. When $\Delta s \in S_{\text{eq}}$, indicating that the space headway is optimal-neither too small nor too large-the ego vehicle adopts the lead vehicle's speed, attenuating oscillations in the lead vehicle's speed through natural attenuation property of cruise control speed tracking.

Note that the AKM model (1) is formulated in continuous-time. For implementation on a physical device, the following discrete-time adaptation is proposed:

$$u_{\text{AKM}}[k+1] = \begin{cases} v_0[k] + \delta_-(\Delta s[k], v_1[k]), & \text{if } \Delta s[k] \in S_-(v_1[k]), \\ \alpha \cdot v_0[k] + (1-\alpha) \cdot u_{\text{AKM}}[k], & \text{if } \Delta s[k] \in S_{\text{eq}}(v_1[k]), \\ v_0[k] + \delta_+(\Delta s[k], v_1[k]), & \text{if } \Delta s[k] \in S_+(v_1[k]), \end{cases} \tag{3}$$

where $\alpha \in (0, 1]$ is a tuning parameter that adjusts the responsiveness of the cruise control's speed tracking. Should the onboard cruise control's speed tracking prove overly responsive, leading to minimal attenuation effects, it is recommended to decrease α towards zero. If this issue does not arise, α should remain at 1.

To demonstrate the integration of the AKM model within standard vehicle control systems, a typical system block diagram is depicted in Fig. 3.

IV. String Stability Analysis

In this section, we establish the local string stability of the proposed controller, illustrating the use of the vehicle's inherent speed tracking to dampen speed oscillations.

Assuming the ego vehicle's cruise control system functions as a proportional controller, the dynamics of the two-vehicle car-following system are described as follows:

$$\dot{v}_1 = k_p(u_{\text{AKM}}(\Delta s, v_0, v_1) - v_1), \tag{4}$$

where $k_p > 0$ represents the proportional gain for velocity tracking. Let $v^* > 0$ represent the desired cruising speed targeted by all vehicles. We define the velocity errors as $e_0 := v_0 - v^*$ and $e_1 := v_1 - v^*$.

TABLE I
Parameters of the Attenuative Kerner's Model

a_1 (m/s^2)	a_2 (m/s^2)	b_1 (m/s)	b_2 (m/s)	d_1 (m/s)	d_2 (m/s)	h_- (s)	h_+ (s)	$v_{\min}$ (m/s)	α –
5.71	1.33	-8.57	-5.33	-5.0	3.0	1.5	4.0	10	0.2

A phase portrait of the system (4), with parameters chosen from Table I and $v_0 \equiv 10$ m / s, is depicted in Fig. 2(b). This phase portrait considers only trajectories originating from feasible initial conditions. The vertical dashed lines divide the space into three segments: from left to right, S_-, S_{eq}, and S_+. Qualitatively, the system exhibits asymptotic convergence to a one-dimensional equilibrium set, indicated by the bold black horizontal line segment $\{(\Delta s, \Delta v) : 15 \le \Delta s \le 40, \Delta v = 0\}$. Additionally, the system converges to the equilibrium set via a sliding surface when within S_+, i.e., when the space headway exceeds 40 m.

Translating the above observation into velocity error dynamics, we find that equilibrium in the coupled velocity error dynamical system occurs when $v_0 = v_1 = v^*$ and $\Delta s \in S_{\text{eq}}(v^*)$, a compact set with a nonempty interior. The dynamics of the coupled error within this equilibrium set are described by:

$$\dot{e}_1 = k_p(e_0 - e_1), \tag{5}$$

forming a linear time-invariant system. Applying the Laplace transform to both sides yields the transfer function:

$$T(s) := \frac{E_1(s)}{E_0(s)} = \frac{k_p}{s + k_p}.$$

As introduced in [8], [13], [18], string stability is a property that describes that a harmonic disturbance experienced by a vehicle driving in equilibrium in a platoon will be attenuated by the subsequent vehicle over time. Following the convention in [33], we formalize the notion of locally string stability below.

Definition 1 (Local String Stability): The system (4) is locally string stable around an equilibrium if $T(s)$ exists and

$$\max_{\forall \omega \in \mathbb{R}} \|T(j\omega)\| \le 1.$$

Next, we show that the controller is locally string stable within the equilibrium set.

Theorem 1: The system (4) is locally string stable for all $k_p > 0$.

Proof: Locally within the equilibrium set of (4), the error dynamical system takes the form of (5). Since $k_p > 0$, the local homogeneous response of (4) is stable, which implies exitence of steady states. Looking at frequency response of the steady state for ω, we have

$$\|T(j\omega)\| = \left\| \frac{k_p}{j\omega + k_p} \right\| = \frac{k_p}{\sqrt{\omega^2 + k_p^2}} \leq 1,$$

for all $\omega \in \mathbb{R}$. By definition, system (4) is locally string stable.■

In fact, for $\omega \neq 0$, we have $\|T(j\omega)\| < 1$, indicating that the controller invariably attenuates nonzero harmonic disturbances. The proof demonstrates that the AKM's second mode consistently acts as an attenuator, attributed to the intrinsic damping effect of cruise control speed tracking. To avert potential collisions or lagging caused by excessive dampening in the second mode, the first and third modes function as headway regulators.

V. Numerical Simulation

To assess the performance of the AKM, we conduct numerical simulations of the model and contrast its outcomes with those from two benchmark approaches: a model of human driver and a model of a commerical ACC.

A. Simulation Setup

Imitating real-world stop-and-go traffic, we consider the lead vehicle's speed to follow an oscillatory profile, defined as

$$v_0^{\text{ref}}(t) = A \sin(\omega t) + B, \tag{6}$$

where $A = 3.35$ m / s, $\omega = \frac{2\pi}{20}$ s $^{-1}$, and $B = 5.59$ m/ s. This profile causes the speed to oscillate between 2.24 m / s (5 mph or 8.05 km / h) and 8.94 m / s (20 mph or 32.19 km / h), achieving a periodicity of 20 seconds.

We selected this harmonic oscillation profile to closely mimic the low-speed stop-and-go waves observed on US highways, while simplifying it to facilitate the comparison of wave attenuation effects. Specifically, we referenced the stop-and-go wave patterns that occur daily during afternoon rush hours on CA State Route 242 near Concord, CA.

We model the vehicle dynamics with a first-order, time-invariant system. This system takes a set speed, u, as input and produces an actuated speed, v, as its output. The dynamics are represented by the equation

$$\dot{v}(t) = k_p(u(t) - v(t)), \tag{7}$$

where, by system identification, k_p is set to 0.32.

Furthermore, for our numerical analysis and subsequent field experiments, we select a specific set of parameters, as detailed in Table I. With the speed profile of the lead vehicle, the dynamics of the ego vehicle, and the controller parameters described above, we can simulate the proposed AKM, enabling it to follow the lead vehicle at the specified speed.

To evaluate the effectiveness of the AKM, we simulate a human driver using the Intelligent Driver Model (IDM) [31], a widely utilized model for representing human driving behavior. Likewise, the Adaptive Cruise Control (ACC) is represented through a modified Optimal Velocity Model (OVM) [13], [17], which is frequently selected for simulating cruise control systems.

To ensure the accuracy of the model, we collect driving data recorded by a human driver and a commercial ACC. We calibrate the human and ACC models by minimizing the discrepancy between the models and the data collected from real-world human and ACC driving, respectively. The calibration procedure, adapted from [6], for a $\mathbf{k}$-parameterized model $f(\mathbf{x} \mid \mathbf{k})$, is presented below:

$$\mathbf{k}^* = \min_{\mathbf{k}, X} w_1 \ell_1(X, \Delta\widehat{S}) + w_2 \ell_2(X, \widehat{V}) + w_3 \ell_3(X) \tag{8a}$$

$$\text{s.t.} \quad \mathbf{x}(0) = \hat{\mathbf{x}}_0 \tag{8b}$$

$$\dot{\mathbf{x}} = \begin{bmatrix} 0 & 1 & 0 & 0 \\ 0 & 0 & 0 & 0 \\ 0 & 0 & 0 & 1 \\ 0 & 0 & 0 & 0 \end{bmatrix} \mathbf{x} + \begin{bmatrix} 0 \\ \dot{\hat{v}}_0(t) \\ 0 \\ f(\mathbf{x} \mid \mathbf{k}) \end{bmatrix}, \tag{8c}$$

where $\mathbf{x} := [s_0 \quad v_0 \quad s_1 \quad v_1]^\top$, $X := \{\mathbf{x}(t) : \forall t \in T\}$, $\Delta\widehat{S} := \{\Delta\hat{s}(t) : \forall t \in T\}$, and $\widehat{V} := \{\hat{v}_1(t) : \forall t \in T\}$ for a specified duration T and

$$\ell_1(X, \Delta\widehat{S}) = \int (\mathbf{x}_1(t) - \mathbf{x}_3(t) - \Delta\hat{s}(t))^2 dt,$$

$$\ell_2(X, \widehat{V}) = \int (\mathbf{x}_4(t) - \hat{v}_1(t))^2 dt,$$

$$\ell_3(X) = \int (\dot{\mathbf{x}}_4(t))^2 dt.$$

Note that we use $\hat{\cdot}$ to distinguish data collected from real-world experiments from data computed from simulations.

The three penalty terms are used for minimizing model-data descrepancy and for model regulation. With $\ell_1(\cdot)$, we penalize the difference between simulated and actual space headway. With $\ell_2(\cdot)$, we penalize the difference between simulated and actual velocity. With $\ell_3(\cdot)$, we penalize large accelerations from the calibrated model to avoid overfitting.

The calibrated IDM for the human driver is

$$a_{\text{HUM}}(\Delta s, v_1, \Delta v) = a \cdot \left(1 - \left(\frac{v_1}{v^*}\right)^{\delta} - \left(\frac{s^*(v_1, \Delta v)}{\Delta s}\right)^2\right), \tag{9}$$

where

$$s^*(v_1, \Delta v) = s_{\min} + v_1 T + \frac{v_1 \Delta v}{2\sqrt{ab}}, \tag{10}$$

with $a = 2.0$ m / s^2, $b = 2.0681$ m / s^2, $\delta = 4$, $T = 0.7254$ s, $s_{\min} = 6.5489$ m, and $v^* = 11.08$ m / s.

The calibrated OVM for commercial ACC is

$$a_{\text{ACC}}(\Delta s, v_1, \Delta v) = k_\alpha(\Delta s + \gamma_1 v_1 + \gamma_0) + k_\beta \Delta v, \tag{11}$$

with $k_\alpha = 0.1222$ s^{-2}, $k_\beta = 2.5094$ s^{-1}, $\gamma_0 = -1.6423$ m, and $\gamma_1 = -0.7925$ s.

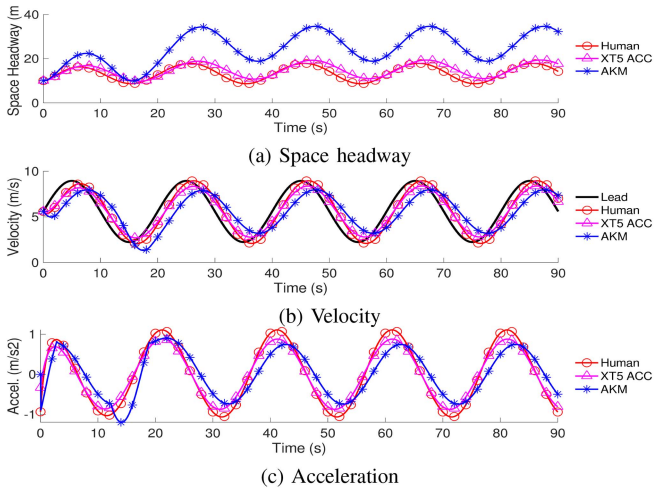

(a) Space headway

(b) Velocity

(c) Acceleration

Fig. 4. Simulated trajectories of the AKM, human driver, and ACC.

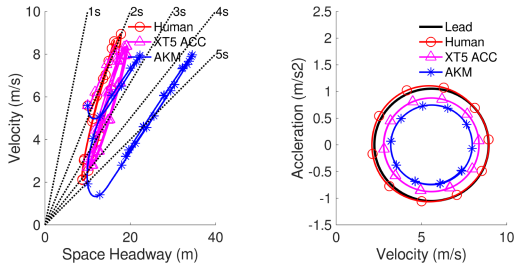

(a) Space Headway - Velocity

(b) Velocity - Acceleration

Fig. 5. Simulated phase portraits of the AKM, human driver, and ACC. The dashed lines in (a) indicate phase motion of different constant time headways.

B. Numerical Results

We simulate the AKM, the human driving model, and the ACC model in low-speed stop-and-go traffic, as characterized by (6). The results are presented as time series in Fig. 4 and as phase portraits in Fig. 5. From Figs. 4 and 5, we observe that

1) The human driving model, as expected, does not reduce the oscillations present in the lead vehicle's trajectory;
2) The ACC model moderately dampens the oscillations in the lead vehicle's trajectory; and
3) The AKM attenuates the oscillations more effectively than the ACC model.

The above observation is particularly evident in Fig. 5(b), where an oscillatory trajectory manifests as a periodic orbit. The more oscillatory the trajectory, the larger the radius of the periodic orbit appears in the phase portrait. As depicted in the plot:

1) The periodic orbit of the human driving model almost coincides with that of the lead vehicle;
2) The periodic orbit of the ACC model is encompassed within that of the lead vehicle; and
3) The periodic orbit of the AKM is situated within that of the ACC model.

Examining the headway plots in Figs. 4(a) and 5(a), we observe that the AKM achieves smoother car-following behavior at the expense of a larger distance between the ego vehicle and the lead vehicle. The human driving model's oscillation occurs within a 2 to 3 s time headway interval; the ACC model oscillates within a 2.5 to 4 s interval; and the AKM model oscillates within a 4 to 5 s interval.

We note that the trade-off between maximum headway and driving smoothness represents the most critical design consideration in developing a wave-dampening controller. The closer a controller is designed to follow the lead vehicle, the smaller the buffer space becomes for mitigating the impacts of stop-and-go behavior exerted by the lead vehicle.

C. Energy Efficiency

Beyond qualitative analysis of the trajectories, it is beneficial to quantitatively compare the three models in terms of their energy consumption efficiency. To this end, we employed an energy consumption model suitable for a typical midsize SUV. This energy model is one of six energy models [12] derived and validated through Autonomie [7], a simulation tool developed by Argonne National Laboratory that includes libraries of different vehicle types.

The model is represented by a function $e(v, a, \theta)$ that maps speed v, acceleration a, and road grade θ to fuel consumption rate e. This empirical model leverages the concept that the instantaneous engine speed N and engine torque T can be directly related to fuel rate. Furthermore, transmission output speed N_{output} and wheel force F_{wheel} are mapped to engine speed and torque. Consequently, both N_{output} and F_{wheel} can be expressed as functions of speed, acceleration, and road grade.

The energy consumption model $e(v, a, \theta)$ is given by

$$e(v, a, \theta) = \max\left\{\ell(v, a, \theta),\ f_{\text{p}}(v, a, \theta)\right\}, \tag{12}$$

where

$$\ell(v, a, \theta) = \begin{cases} \beta, & \text{if } v \le v_{\text{c}}, \\ 0, & \text{if } v > v_{\text{c}} \text{ and } a < a_{\text{c}}(v, \theta), \end{cases}$$

$$f_{\text{p}}(v, a, \theta) = C(v) + P(v)a + Q(v)(a_+)^2 + Z(v)\theta\ .$$

The function $f_{\text{p}}(v, a, \theta)$ denotes the fuel rate and is a polynomial function of speed v, acceleration a, and road grade θ. The term $\ell(v, a, \theta)$ serves as a lower bound for the fuel rate consumed by the vehicle. The critical speed for fuel-cut activation is denoted by v_{c}, while the acceleration threshold for fuel-cut, dependent on speed and road grade, is defined by the polynomial $a_{\text{c}}(v, \theta)$. The coefficients $C(v)$, $P(v)$, and $Q(v)$ are polynomial functions of speed designed to ensure that $f_{\text{p}}(v, a, 0)$ is monotonically increasing with respect to a, by setting a constraint that the minimum $f_{\text{p}}(v, a_{\min}(v), 0)$ remains positive.

Despite its simplicity, this energy consumption model facilitates the convenient calculation of the vehicle's fuel consumption rate in grams-per-second of *gasoline*. In this section and the subsequent ones, we assume the road grade to be zero, as this represents the most common scenario in the real world. Utilizing this energy consumption model, we compute the energy efficiency of the three car-following models. Sorting the efficiency of the three models in ascending order yields the fuel

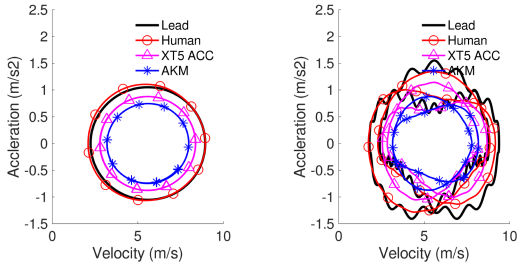

(a) Without disturbances (b) With disturbances

Fig. 6. Evaluation of the impacts of disturbances on AKM. The qualitive efficiency ranking of these models remain unchanged.

rate of the human driver 0.5697 g / s, the ACC 0.5090 g / s, and the most efficient AKM 0.4900 g / s. This quantitative result aligns with the qualitative analysis presented earlier.

D. Robustness to Disturbances

Because human drivers never adheres to the idealistic sinusoidal velocity in (6), we further examine the performance of all models under a more realistic velocity profile with disturbances. To emulate real-world disturbances, we have augmented (6) with two additional harmonic waves, as shown below:

$$v_0^{\text{ref}}(t) = A_1 \sin(\omega_1 t) + A_2 \sin(\omega_2 t) + A_3 \sin(\omega_3 t) + B, \tag{13}$$

where $A_1 = 3.35$m/s, $A_2 = 0.509$m/s, $A_3 = 0.0159$m/s, $\omega_1 = \frac{2\pi}{20}$ s^{-1}, $\omega_2 = \frac{2\pi}{8}$ s^{-1}, $\omega_3 = 2\pi$ s^{-1}, and $B = 5.59$m/s.

Simulations with this disturbed velocity profile have yielded largely consistent results. The acceleration-velocity phase portrait, illustrating the robustness of our method, is displayed in Fig. 6. Again sorting the efficiency of the three models, the fuel rates are as follows: the human driver at 0.5695g / s, the ACC at 0.5095g/ s, and the most efficient AKM at 0.4881g/ s. As demonstrated, the performance of the AKM does not deteriorate under disturbances, suggesting its robustness to such conditions.

VI. Physical Experiments

Given that sensing and actuation in actual vehicles are typically far from perfect [2], [24], verifying the performance of a controller in a real vehicle is crucial to attest its robustness. Unlike most prior studies, we conducted field experiments to validate the performance of our proposed AKM method. To achieve this, we customized a 2022 Cadillac XT5 and carried out the same set of experiments as described in the simulation on this custom SUV.

A. Experimental Setup

To achieve this goal, we deployed the AKM model on a 2022 Cadillac XT5, as illustrated in Fig. 7(a). To interface with the vehicle, we utilized a commericial CAN bus transceiver named neoVI FIRE2 serving as the interface device to query sensor estimates and issue actuation commands. A trunk view of the hardware integration is shown in Fig. 7(b). The XT5 is configured to accept velocity commands, in accordance with the block diagram presented in Fig. 3. This customization allows the vehicle to track both constant and variable velocity inputs provided by the AKM.

(a) Angled view (b) Trunk view

Fig. 7. An angled view and a trunk view of the automated Cadillac XT5.

Fig. 8. Satellite image of the experiment site in Richmond, CA, USA.

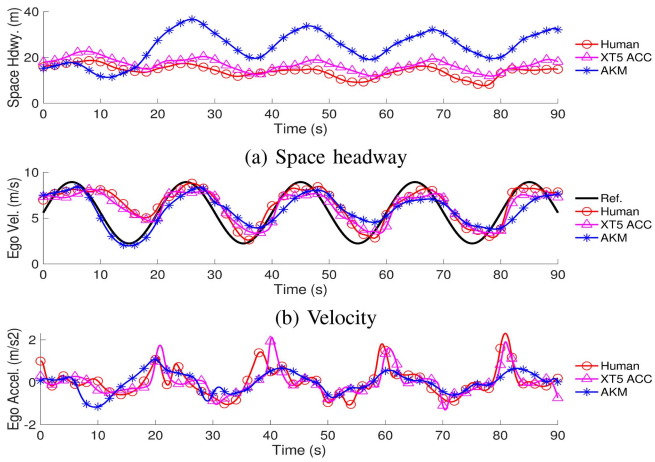

(a) Space headway

(b) Velocity

(c) Acceleration

Fig. 9. Measured trajectories of the AKM, human driver, and ACC.

The experiments were conducted at the Richmond Field Station in California, US, as illustrated by the satellite image in Fig. 8. The test track starts at the exit of the left parking lot and concludes at the entrance of the right parking lot, spanning a total length of approximately 640 meters. In each test, a lead human driver was tasked with adhering as closely as possible to the velocity profile specified in (6). Simultaneously, the ego vehicle, under the supervision of a safety driver, followed the lead vehicle employing either manual driving, the onboard ACC, or the AKM. To account for variations in human execution of the lead reference trajectory, we conducted five repeated runs for each of the three car-following modes.

B. Experimental Results

Sample trajectories of human driving, the XT5 ACC, and the AKM are depicted in Figs. 9 and 10. When comparing the experimental results to those from simulations, we observe that

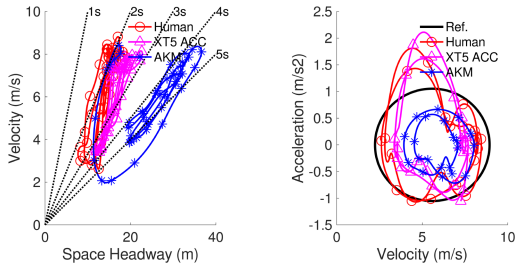

(a) Space headway - velocity (b) Velocity - acceleration

Fig. 10. Measured phase portraits of the AKM, human driver, and ACC.

TABLE II
MEASURED FUEL RATES (G/S GASOLINE) IN THE PHYSICAL EXPERIMENTS

	Run 1	Run 2	Run 3	Run 4	Run 5	Mean
Human	0.5182	0.5134	0.5136	0.5277	0.5277	0.5201
XT5 ACC	0.5043	0.4748	0.4874	0.4424	0.4472	0.4712
AKM	0.4246	0.4270	0.4450	0.4324	0.4167	0.4291

the high-level car-following characteristics of the three methods remain consistent: human driving exhibits the least effectiveness in wave dampening; the AKM performs the best; and the XT5 ACC ranks in the middle.

The primary distinction between numerical simulations and physical experiments lies in the inability of the human driving and ACC models to replicate short bursts of acceleration, as evidenced in Fig. 9(c). This suggests that, in practice, both actual human driving and the XT5 ACC adopt a more aggressive approach towards closing any significant gaps between the ego vehicle and the lead vehicle, compared to their simulated counterparts.

C. Energy Efficiency

Utilizing the energy consumption model presented in (12), we can further qualitatively evaluate the efficiency of the three car-following methods. The fuel consumption rates for each method across all test runs are succinctly summarized in Table II. Analysis of the data reveals that although the numerical values differ from those obtained in simulations, the relative order of energy efficiency remains consistent: the AKM is the most efficient; human driving is the least efficient; and the XT5 ACC occupies the middle ground.

VII. DISCUSSION

Before concluding, we want to remark on several important theoretical and practical aspects of our works.

A. Theoretical Remarks

In Section IV, we presented a qualitative illustration of the global convergence property to an equilibrium set and the local string stability of the AKM within that equilibrium set. However, a proof of such convergence and an examination of global string stability remain pending. Given that the full system exhibits piecewise affine characteristics, rendering it nonlinear, traditional approaches for linear systems are inapplicable. This complexity makes the analysis challenging.

To demonstrate global convergence to the equilibrium set, we must carefully analyze the transitions among the three jump sets S_-, S_{eq}, and S_+. Alternatively, we could attempt to numerically solve for a Lyapunov function using the procedure described in [10].

To probe into the string stability of this nonlinear dynamic system, a potential avenue is to assess the bounded-input-bounded-output (BIBO) stability of the error dynamics. Beyond BIBO stability, it is imperative to also demonstrate that error propagation behaves as a contraction map. Pursuing these two propositions necessitates exploring outside the confines of linear systems theory.

B. Practical Considerations

First and foremost, we emphasize the necessity of precise calibration of AKM parameters, including a_1, a_2, h_-, h_+, and α. In scenarios where the ACC exhibits sluggishness due to delays or quantization, adjustments to a_1, a_2, h_-, h_+ are critical to optimize response characteristics. Specifically, if the vehicle tends to drive too close to the lead vehicle, one should consider decreasing a_1 while increasing h_-. Conversely, if the vehicle consistently lags behind the lead vehicle, increasing a_2 while decreasing h_+ should be considered. In the second mode, where the ACC response to reference speed is overly rapid, reducing α will improve the dampening effect. Lastly, imposing additional constraints on u_{AKM} may be required to maintain speed commands within legal limits.

When operating on highways, it is essential to consider the potential side effects of increased space headway due to the AKM. A primary disadvantage of increased space headway is the resultant decrease in traffic flow density, particularly during rush hours. Consequently, this reduction may lead to decreased highway capacity, potentially causing greater congestion on local roads and highway onramps. Another shortcoming occurs when the AKM activates in traffic flows where the density is below the critical threshold, potentially reducing overall traffic throughput. However, this scenario is unlikely since stop-and-go waves typically occur above the critical density.

Furthermore, we acknowledge that our model does not account for two critical scenarios, which require human intervention. The first involves the lead vehicle initiating an emergency stop. Under such circumstances, we expect human drivers to intervene promptly by applying brakes to avert a collision. The second scenario occurs when the lead vehicle accelerates beyond the speed limit and exits the radar sensors' detection range. To prevent the following vehicle from engaging in unsafe pursuit, we recommend that a human driver take over or that supplementary measures be incorporated.

Lastly, we comment on the most salient practical challenges encountered during the project. Among these, customizing the Cadillac XT5 for automated driving presented significant difficulties. Part of the challenge stemmed from developing the driver to interface with the vehicle CAN buses. Additionally, mastering the temporal requirements of each CAN bus signal

proved complex: certain signals must be transmitted at specific times or frequencies to be registered by the CAN buses. Another challenge involved designing experiments with the appropriate level of complexity to demonstrate the effectiveness of our method. Conducting full-scale field tests on highways introduced too many variables, complicating the isolation of our controller's impacts. Instead, emulating repeatable highway scenarios in controlled environments struck an optimal balance between complexity and control.

VIII. Conclusion

In this letter, we introduce a general velocity-based controller termed the Attenuative Kerner's Model (AKM). We evaluate AKM against a human driver and commercial Adaptive Cruise Control using both numerical simulations and physical experiments. Our analysis indicates that AKM maintains local string-stability within the equilibrium set. Results from simulations and experiments demonstrate that in low-speed stop-and-go traffic, AKM outperforms both the human driver and ACC in terms of smoother car-following and enhanced energy efficiency.

Acknowledgment

Any opinions, findings, and conclusions or recommendations expressed in this material are those of the author(s) and do not necessarily reflect the views of the National Science Foundation. The views expressed herein do not necessarily represent the views of the U.S. Department of Energy or the United States Government.

References

[1] E. Benedito, A. Doria-Cerezo, C. Kunusch, and J. M. Olm, "Traffic flow-oriented design and analysis of an adaptive cruise control system," in *2018 IEEE Int. Symp. Circuits Syst.*, 2018, pp. 1–5.

[2] R. Bhadani et al., "Real-time distance estimation and filtering of vehicle headways for smoothing of traffic waves," in *Proc. 10th ACM/IEEE Int. Conf. Cyber- Phys. Syst.*, 2019, pp. 280–290.

[3] M. R. Flynn, A. R. Kasimov, J.-C. Nave, R. R. Rosales, and B. Seibold, "Self-sustained nonlinear waves in traffic flow," *Phys. Rev. E*, vol. 79, May 2009, Art. no. 056113.

[4] D. Gloudemans et al., "I-24 motion: An instrument for freeway traffic science," *Transp. Res. Part C, Emerg. Technol.*, vol. 155, 2023, Art. no. 104311.

[5] A. L. Gratzer, S. Thormann, A. Schirrer, and S. Jakubek, "String stable and collision-safe model predictive platoon control," *IEEE Trans. Intell. Transp. Syst.*, vol. 23, no. 10, pp. 19358–19373, Oct. 2022.

[6] G. Gunter et al., "Are commercially implemented adaptive cruise control systems string stable?," *IEEE Trans. Intell. Transp. Syst.*, vol. 22, no. 11, pp. 6992–7003, Nov. 2021.

[7] S. Halbach, P. Sharer, S. Pagerit, A. P. Rousseau, and C. Folkerts, "Model architecture, methods, and interfaces for efficient math-based design and simulation of automotive control systems," SAE Tech. Paper, Tech. Rep. 2010-01-0241, 2010.

[8] P. Ioannou and Z. Xu, "Throttle and brake control systems for automatic vehicle following," *IVHS J.*, vol. 1, no. 4, pp. 345–377, 1994.

[9] L. Jiang, Y. Xie, X. Wen, D. Chen, T. Li, and N. G. Evans, "Dampen the stop-and-go traffic with connected and automated vehicles–A deep reinforcement learning approach," in *2021 7th Int. Conf. Models Technol. Intell. Transp. Syst.*, 2021, pp. 1–6.

[10] M. Johansson and A. Rantzer, "Computation of piecewise quadratic Lyapunov functions for hybrid systems," in *1997 Eur. Control Conf.*, 1997, pp. 2005–2010.

[11] B. S. Kerner, "Physics of automated driving in framework of three-phase traffic theory," *Phys. Rev. E*, vol. 97, no. 4, 2018, Art. no. 042303.

[12] N. Khoudari et al., "Reducing detailed vehicle energy dynamics to physics-like models," 2023, *arXiv:2310.06297*.

[13] C. Y. Liang and H. Peng, "Optimal adaptive cruise control with guaranteed string stability," *Veh. Syst. Dyn.*, vol. 32, no. 4/5, pp. 313–330, 1999.

[14] N. Lichtlé, E. Vinitsky, M. Nice, B. Seibold, D. Work, and A. M. Bayen, "Deploying traffic smoothing cruise controllers learned from trajectory data," in *2022 Int. Conf. Robot. Automat.*, 2022, pp. 2884–2890.

[15] B. Coifman, D. Beymer, P. McLauchlan, and J. Malik, "A real-time computer vision system for vehicle tracking and traffic surveillance," *Transp. Res. Part C: Emerg. Technol.*, vol. 6, no. 4, pp. 271–288, 1988.

[16] S. T. McQuade et al., "Medium-scale to large-scale implementation of cyber-physical human experiments in live traffic," *IFAC-PapersOnLine*, vol. 55, no. 41, pp. 83–88, 2022.

[17] V. Milanés, S. E. Shladover, J. Spring, C. Nowakowski, H. Kawazoe, and M. Nakamura, "Cooperative adaptive cruise control in real traffic situations," *IEEE Trans. Intell. Transp. Syst.*, vol. 15, no. 1, pp. 296–305, Feb. 2014.

[18] G. J. L. Naus, R. P. A. Vugts, J. Ploeg, M. J. G. van De Molengraft, and M. Steinbuch, "String-stable CACC design and experimental validation: A frequency-domain approach," *IEEE Trans. Veh. Technol.*, vol. 59, no. 9, pp. 4268–4279, Nov. 2010.

[19] L. Ng, C. M. Clark, and J. P. Huissoon, "Reinforcement learning of dynamic collaborative driving Part I: Longitudinal adaptive control," *Int. J. Veh. Inf. Commun. Syst.*, vol. 1, no. 3/4, pp. 208–228, 2008.

[20] M. Nice, M. Bunting, G. Gunter, W. Barbour, J. Sprinkle, and D. Work, "Sailing CAVs: Speed-adaptive infrastructure-linked connected and automated vehicles," 2023, *arXiv:2310.06931*.

[21] X. Qu, Y. Yu, M. Zhou, C.-T. Lin, and X. Wang, "Jointly dampening traffic oscillations and improving energy consumption with electric, connected and automated vehicles: A reinforcement learning based approach," *Appl. Energy*, vol. 257, 2020, Art. no. 114030.

[22] R. Rajamani and S. E. Shladover, "An experimental comparative study of autonomous and co-operative vehicle-follower control systems," *Transp. Res. Part C, Emerg. Technol.*, vol. 9, no. 1, pp. 15–31, 2001.

[23] A. E. L. Rharbali, H. Bousfiha, M. Hasri, and Y. Salih-Alj, "Smart cruise control system with Stop&Go and predictive road mapping," in *2012 8th IEEE Int. Symp. Instrum. Control Technol.*, 2012, pp. 116–121.

[24] M. Segata, R. L. Cigno, R. K. Bhadani, M. Bunting, and J. Sprinkle, "A lidar error model for cooperative driving simulations," in *2018 IEEE Veh. Netw. Conf.*, 2018, pp. 1–8.

[25] E. Solano-Araque, G. Colin, G.-M. Cloarec, A. Ketfi-Cherif, and Y. Chamaillard, "Determining vehicle acceleration from noisy non-uniformly sampled speed data for control purposes," *IFAC-PapersOnLine*, vol. 52, no. 5, pp. 66–71, 2019.

[26] R. E. Stern et al., "Quantifying air quality benefits resulting from few autonomous vehicles stabilizing traffic," *Transp. Res. Part D, Transport Environ.*, vol. 67, pp. 351–365, 2019.

[27] R. E. Stern et al., "Dissipation of stop-and-go waves via control of autonomous vehicles: Field experiments," *Transp. Res. Part C, Emerg. Technol.*, vol. 89, pp. 205–221, 2018.

[28] Y. Sugiyama et al., "Traffic jams without bottlenecks-experimental evidence for the physical mechanism of the formation of a jam," *New J. Phys.*, vol. 10, no. 3, 2008, Art. no. 033001.

[29] J. Sun, Z. Zheng, and J. Sun, "The relationship between car following string instability and traffic oscillations in finite-sized platoons and its use in easing congestion via connected and automated vehicles with IDM based controller," *Transp. Res. Part B, Methodological*, vol. 142, pp. 58–83, 2020.

[30] D. Swaroop and J. K. Hedrick, "String stability of interconnected systems," *IEEE Trans. Autom. control*, vol. 41, no. 3, pp. 349–357, Mar. 1996.

[31] M. Treiber, A. Hennecke, and D. Helbing, "Congested traffic states in empirical observations and microscopic simulations," *Phys. Rev. E*, vol. 62, no. 2, 2000, Art. no. 1805.

[32] M. Wang, W. Daamen, S. P. Hoogendoorn, and B. Van Arem, "Connected variable speed limits control and car-following control with vehicle-infrastructure communication to resolve stop-and-go waves," *J. Intell. Transp. Syst.*, vol. 20, no. 6, pp. 559–572, 2016.

[33] C. Wu, A. M. Bayen, and A. Mehta, "Stabilizing traffic with autonomous vehicles," in *2018 IEEE Int. Conf. Robot. Automat.*, 2018, pp. 6012–6018.

[34] C. Wu, A. R. Kreidieh, K. Parvate, E. Vinitsky, and A. M. Bayen, "Flow: A modular learning framework for mixed autonomy traffic," *IEEE Trans. Robot.*, vol. 38, no. 2, pp. 1270–1286, Apr. 2022.

[35] F. Wu and A. M. Bayen, "A hierarchical MPC approach to car-following via linearly constrained quadratic programming," *IEEE Control Syst. Lett.*, vol. 7, pp. 532–537, 2023.

[36] F. Wu et al., "Decentralized vehicle coordination: The Berkeley deepdrive drone dataset," 2022, *arXiv:2209.08763*.